Atmospheric Environment 155 (2017) 129–139

Contents lists available at ScienceDirect

Atmospheric Environment

journal homepage: www.elsevier.com/locate/atmosenv

Spatiotemporal prediction of continuous daily $PM_{2.5}$ concentrations across China using a spatially explicit machine learning algorithm

Yu Zhan [a], Yuzhou Luo [b], Xunfei Deng [c], Huajin Chen [b], Michael L. Grieneisen [b], Xueyou Shen [a], Lizhong Zhu [a, *], Minghua Zhang [b, **]

[a] *Department of Environmental Science, Zhejiang University, Hangzhou, Zhejiang 310058, China*
[b] *Department of Land, Air, and Water Resources, University of California, Davis, CA 95616, USA*
[c] *Institute of Digital Agriculture, Zhejiang Academy of Agricultural Sciences, Hangzhou, Zhejiang 310021, China*

HIGHLIGHTS

- A novel machine learning model for predicting daily $PM_{2.5}$ concentrations in China.
- This model shows superior predictive performance and is able to handle missing data.
- >90% of the population lived in areas with annual mean $PM_{2.5}$ > 35 μg/m3
- >40% of the population was exposed to $PM_{2.5}$ >75 μg/m3 for over 100 days in a year.

GRAPHICAL ABSTRACT

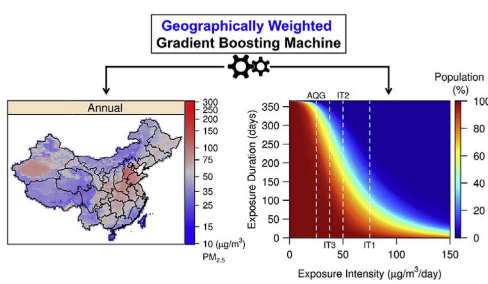

ARTICLE INFO

Article history:
Received 16 December 2016
Received in revised form
8 February 2017
Accepted 10 February 2017
Available online 15 February 2017

Keywords:
Fine particulate matter
Human exposure
Spatial nonstationarity
Geographically weighted
Machine learning

ABSTRACT

A high degree of uncertainty associated with the emission inventory for China tends to degrade the performance of chemical transport models in predicting $PM_{2.5}$ concentrations especially on a daily basis. In this study a novel machine learning algorithm, Geographically-Weighted Gradient Boosting Machine (GW-GBM), was developed by improving GBM through building spatial smoothing kernels to weigh the loss function. This modification addressed the spatial nonstationarity of the relationships between $PM_{2.5}$ concentrations and predictor variables such as aerosol optical depth (AOD) and meteorological conditions. GW-GBM also overcame the estimation bias of $PM_{2.5}$ concentrations due to missing AOD retrievals, and thus potentially improved subsequent exposure analyses. GW-GBM showed good performance in predicting daily $PM_{2.5}$ concentrations ($R^2 = 0.76$, RMSE = 23.0 μg/m3) even with partially missing AOD data, which was better than the original GBM model ($R^2 = 0.71$, RMSE = 25.3 μg/m3). On the basis of the continuous spatiotemporal prediction of $PM_{2.5}$ concentrations, it was predicted that 95% of the population lived in areas where the estimated annual mean $PM_{2.5}$ concentration was higher than 35 μg/m3, and 45% of the population was exposed to $PM_{2.5}$ >75 μg/m3 for over 100 days in 2014. GW-GBM accurately predicted continuous daily $PM_{2.5}$ concentrations in China for assessing acute human health effects.

1. Introduction

Exposure to fine particulate matter with diameter <2.5 μm ($PM_{2.5}$) has been associated with increased cardiovascular

* Corresponding author.
** Corresponding author.
E-mail addresses: zlz@zju.edu.cn (L. Zhu), mhzhang@ucdavis.edu (M. Zhang).

http://dx.doi.org/10.1016/j.atmosenv.2017.02.023

morbidity and respiratory mortality (Dockery et al., 1993; Keller et al., 2015; Madaniyazi et al., 2015; Pope et al., 2011; Puett et al., 2009), as well as decreased birth weight (Rich et al., 2015). Annual average daily $PM_{2.5}$ exposure levels have been used to develop exposure-response functions (Burnett et al., 2014), and to assess the Global Burden of Disease or mortality attributable to ambient $PM_{2.5}$ (Apte et al., 2015; Brauer et al., 2012). In addition, reliable daily $PM_{2.5}$ exposure levels are needed to assess acute health effects (Shang et al., 2013), such as acute lower respiratory infection for children. China is one of the countries with the most severe air pollution by $PM_{2.5}$ (Brauer et al., 2016; Lai et al., 2013). Severe $PM_{2.5}$ pollution has attracted public attention, and the Chinese government has been implementing regulations which aim to achieve a 15–25% decrease of $PM_{2.5}$ concentrations from 2012 to 2017 for highly polluted areas (SCPRC, 2013). While the air quality monitoring network has covered most major cities in China (MEPC, 2015), nationwide spatiotemporal distributions of $PM_{2.5}$ concentrations should be delineated for human exposure assessment and policy making.

Various models have been developed for predicting the spatiotemporal distributions of $PM_{2.5}$ concentrations, including chemical transport models (CTMs) and statistical models.

On the basis of meteorological fields generated by climate models, CTMs simulate main processes of chemicals in the atmosphere, including emissions, chemistry, transport, and deposition (Jacob, 1999). For instance, the Goddard Earth Observing System-chemical transport (GEOS-Chem) model (Bey et al., 2001), is able to predict compositions and concentrations of $PM_{2.5}$ based on the corresponding emission inventories and environmental conditions (Geng et al., 2015; van Donkelaar et al., 2016). This model is especially valuable for regions without $PM_{2.5}$ monitoring data, where statistical models are generally inapplicable. This model showed good predictive performance when assimilated with satellite-retrieved aerosol optical depth (AOD), and even better performance when ground-based $PM_{2.5}$ observations were also incorporated (van Donkelaar et al., 2016). Nevertheless, CTM's performance could be undermined by high uncertainty in the emission inventories presented on a fine spatiotemporal resolution (e.g., $1° \times 1°$ grids and daily). This is especially true for China, where the amount of annual coal consumption has been corrected up to 12% higher than previously reported (NBSC, 2013; 2015).

Given the established monitoring network in China, sophisticated statistical models that do not rely on the emission inventories tend to be more suitable for predicting spatiotemporal distributions of $PM_{2.5}$ concentrations in China on a fine spatiotemporal resolution. A number of statistical models, such as the geographically weighted regression (GWR) model (Ma et al., 2014), the mixed-effect models (Ma et al., 2016a; Xie et al., 2015), and the Bayesian hierarchical model (Lv et al., 2016), have been adopted to predict the $PM_{2.5}$ concentrations in China. These statistical models predict spatiotemporal distributions of $PM_{2.5}$ based on the ground-based $PM_{2.5}$ observations, AOD satellite retrievals, meteorological conditions, and/or land use types. In dealing with missing data, these statistical models generally employ interpolation to fill missing AOD retrievals or simply exclude the data points (i.e., data records) with missing values (Kloog et al., 2011; Lv et al., 2016; Ma et al., 2016a). The exclusion however tends to result in biased estimates of $PM_{2.5}$ concentrations (Geng et al., 2015; van Donkelaar et al., 2010). These biased estimates tend to degrade the associated epidemiological analysis, such as the Global Burden of Disease (Naghavi et al., 2015). Although complete sets of AOD retrievals can be developed by fusing the data from different satellites or through interpolation (Nguyen et al., 2012; Xu et al., 2015), the change-of-support problem (i.e., inconsistent spatial units) or the propagation of uncertainty in interpolation are likely to emerge. In addition, these statistical models that belong to the data modeling culture assume that the observations are generated by specified stochastic models (Breiman, 2001). Nevertheless, the specified models are likely to oversimplify the otherwise complex relationships between $PM_{2.5}$ concentrations and the predictor variables (Reid et al., 2015), such as by ignoring effects of interaction between predictor variables on $PM_{2.5}$ or nonlinear relationships between predictor variables and $PM_{2.5}$.

Machine learning algorithms or models, which pertain to the algorithmic modeling culture, learn model structures from training data and generally show better predictive performance than conventional statistical models (Breiman, 2001; Hastie et al., 2009). For instance, a neural network model with a good performance was developed to predict the daily $PM_{2.5}$ concentrations in the continental United States (Di et al., 2016). A gradient boosting machine (GBM) model outperformed ten other statistical models in predicting the $PM_{2.5}$ concentrations in California after a major fire event (Reid et al., 2015). A GBM model, with the strengths of classification/regression trees and boosting, grows an ensemble of weak decision trees in a forward and stage-wise fashion (Friedman, 2001, 2002). By learning from training data, GBM models are able to capture interaction and nonlinearity in dependence structures, as well as to handle missing data in a data point, such as missing AOD retrieval. However, a "global" model is unable to address the spatial nonstationarity in the relationship between $PM_{2.5}$ concentrations and predictor variables. Moreover, trend-fitting methods such as spline interpolation or Kriging are inadequate to capture complex spatial variation (Brunsdon et al., 1996). Thus, the model structure should alter geographically to reflect the spatial nonstationarity.

This study aims to develop a spatially explicit GBM model, named Geographically Weighted (GW) GBM, for predicting the continuous daily $PM_{2.5}$ concentrations across China. Spatial smoothing kernels were adopted to model the spatial nonstationarity in the relationship between $PM_{2.5}$ concentrations and predictor variables. The GW-GBM model was used to predict the daily $PM_{2.5}$ concentrations for 2014 in China ($0.5° \times 0.5°$ grids were used due to the high computational expense of the GW-GBM model) based on the ground-based $PM_{2.5}$ observations, AOD data from the Aqua-retrieved Collection 6 of Moderate-resolution Imaging Spectroradiometer (MODIS) aerosol products (Levy et al., 2013), and meteorological conditions. The predictive performance of the GW-GBM model was evaluated by using cross-validation. We then evaluated the estimation bias of $PM_{2.5}$ concentrations due to missing AOD retrievals, as well as the interaction, nonlinearity, and spatial nonstationarity of the dependence structure of $PM_{2.5}$ on the predictor variables. The GW-GBM model with good predictive performance and capable of dealing with missing data is expected to advance the $PM_{2.5}$ modeling.

2. Materials and methods

2.1. Data preparation

The GW-GBM model was used to predict the daily $PM_{2.5}$ concentrations in 2014 at $0.5° \times 0.5°$ spatial resolution for China (4 194 grid cells) based on the ground-based $PM_{2.5}$ monitoring data (Fig. S1), day of year (DOY), AOD, and meteorological conditions. The $PM_{2.5}$ monitoring data were retrieved from the National Air Quality Monitoring Network for mainland China and Hainan Island (MEPC, 2015), the Environmental Protection Department of Hong Kong (http://www.epd.gov.hk) for Hong Kong, and the Environmental Protection Administration of Taiwan (http://taqm.epa.gov.tw) for Taiwan. The $PM_{2.5}$ concentrations were measured with either the tapered element oscillating microbalance technology or the beta-attenuation method (Zhao et al., 2016). The monitoring sites with less than half-year data were excluded from this analysis. The $PM_{2.5}$ monitoring data for 1 015 sites from 267 cities were obtained, which were assigned to their enclosing grid cells. Averages were taken for the cells containing multiple monitoring sites, resulting in 285 grid cells with $PM_{2.5}$ monitoring data.

The AOD data were obtained from the deep blue/dark target merged product contained in the Aqua-retrieved Collection 6 MODIS aerosol products at level 2 (Levy et al., 2013). Although 1×1 km^2 AOD products were available from the Multi-Angle Implementation of Atmospheric Correction (MAIAC) algorithm (Lyapustin et al., 2011), these AOD products were not completed for China in 2014 at the time of this study. The AOD data were resampled to the delineated grids by averaging. The overall percentage of missing AOD was 39.1% (Table S1). The daily meteorological conditions, including air temperature, atmospheric pressure, evaporation, precipitation, relative humidity, sunshine duration, and wind speed, for 839 meteorological stations were downloaded from the China Meteorological Data Center (http://data.cma.cn). The elevation data, with a resolution of 90 m at the equator, were obtained from the Shuttle Radar Topography Mission (SRTM) database (Jarvis et al., 2008). These site-specific meteorological data were interpolated to the delineated grids using co-Kriging with normal score transformation (Deutsch and Journel, 1998), where elevation data were incorporated into the estimator. The gridded population density data, with a resolution of 1 km, were obtained from the Data Center for Resources and Environmental Sciences for calculating population-weighted $PM_{2.5}$ concentrations (RESDC, 2014), which were resampled to the delineated grids by averaging. Note that all data were summarized in the delineated grids used for model development, evaluation, and prediction.

2.2. Model description

The GW-GBM model was developed as an ensemble of GBM models, where a single GBM model, hereafter referred to as a sub-model, was used for each predicting cell at $0.5° \times 0.5°$ resolution. Each GW-GBM sub-model was trained to optimize a weighted squared error loss function for the associated training cells (Ridgeway, 2015):

$$L(y, f(x)) = \sum_{m=1}^{M}\sum_{n=1}^{N_m} w_m [y_{mn} - f(x_{mn})]^2 \Big/ \sum_{m=1}^{M} (w_m N_m) \tag{1}$$

where $L(y, f(x))$ is the loss function for predicting observation y (i.e., $PM_{2.5}$ concentrations) by model $f(x)$; x represents predictor variables, including DOY, AOD, atmospheric pressure, air temperature, evaporation, wind speed, relative humidity, sunshine duration, and precipitation; m is a running index for the training cells ($m = 1$ to M; M is the total number of training cells, i.e., cells with $PM_{2.5}$ monitoring data); n is a running index for the data points from cell m ($n = 1$ to N_m; N_m is the total number of data points from cell m); x_{mn} and y_{mn} are values of predictor and response variables, respectively, for data point mn; and w_m is the weight of training cell m, which is determined by the spatial smoothing kernel based on the distance between this training cell and the predicting cell. The strategy for identifying training cells for a targeted predicting cell, as well as the formulas for three commonly adopted spatial smoothing kernels (i.e., Gaussian, bisquare, and tricube), are listed in the Supplement S2.

The loss function (Eq. (1)) was optimized through the GBM procedure (Friedman, 2001, 2002). Please see Supplement S1 for more reader-friendly explanations of the following steps.

$$\text{Initialization}: \; f_0(x) = \sum_{m=1}^{M}\sum_{n=1}^{N_m}(w_m y_{mn}) \Big/ \sum_{m=1}^{M}(w_m N_m) \tag{2}$$

For $k = 1$ to K:

$$\text{Subsampling}: \; \{j\}_1^S = sample\left(\{i\}_1^{N_T}, S\right) \tag{3}$$

$$\text{Updating residuals}: \; \tilde{y}_j = y_j - f_{k-1}(x_j) \tag{4}$$

$$\text{Growing a tree}: \; \{R_{lk}\}_1^L = tree\left(\left\{\tilde{y}_j, x_j\right\}_1^S\right) \tag{5}$$

$$\text{Computing terminal node prediction}: \; \rho_{lk} = \sum_{x_j \in R_{lk}}\left(w_j \tilde{y}_j\right) \Big/ \sum_{x_j \in R_{lk}} w_j \tag{6}$$

Shrinking the new tree and adding it to the model:

$$f_k(x) = f_{k-1}(x) + \lambda \rho_{lk} I(x \in R_{lk}) \tag{7}$$

where at each step k, a subsample with S data points $\{j\}_1^S$ are drawn from the training dataset $\{i\}_1^{N_T}$ at random without replacement ($N_T = \sum_{m=1}^{M} N_m$); $\tilde{y}_j$ is the pseudo residual produced by the model updated at the previous step annotated as $f_{k-1}(x_j)$; R_{lk} represents the region of the predictor feature space corresponding to terminal l of the new tree with L terminals; ρ_{lk} is the prediction for terminal l; w_j is the weight of the cell that contains data point j; and λ is the shrinkage rate ($\lambda = 0.05$). In growing a tree (step 5), it starts with a single (root) node, and then searches over all binary splits of all predictor variables for the one that reduces the weighted squared error loss the most. The tree-split process iterates until the minimum number of data points in a terminal node (default: 10) or the maximum tree depth is reached. The tree depth (i.e., interaction depth) is the length of the longest path from the root to the terminal nodes, which reflects the interaction among the predictor variables. For example, a tree depth of 1 implies an additive model, and a depth of 2 implies 2-way interactions.

Note that K is determined with sample-based 10-fold cross-validation, where the training samples are randomly partitioned into 10 groups of approximately the same size (Elith et al., 2008). Starting with a selected K' (e.g., 50), the GW-GBM model trained with 9 groups makes predictions for the remaining group, which is repeated 10 times to obtain a complete set of predictions, and the root-mean-square error (RMSE) is recorded. This process is repeated with a larger K' until the RMSE does not decrease for 5 steps. K is set to the optimal K' and is used to train the formal GW-GBM model.

2.3. Missing data handling

As a tree-based model, the GW-GBM model can handle missing data for continuous predictor variables by using surrogate splits (Breiman et al., 1984). In growing trees, primary splits were first determined by using the subset of data with complete records for each partially missing variable. Then, a list of surrogate predictor variables and split points (namely surrogate splits) were formed, which produce splits similar to the primary splits. When making predictions based on the data points with missing records of a given variable, the surrogate splits were chosen in the order of their similarity to the primary splits in case some surrogate splits are still unavailable due to missing data.

2.4. Model prediction

The continuous daily $PM_{2.5}$ concentrations for China in 2014 were predicted on the 0.5° × 0.5° grids using the GW-GBM model. Seven regions of China were used for spatially summarizing model predictions, including North, Northwest, Northeast, East, Central, South, and Southwest China (Fig. S1). The annual and quarterly averages of $PM_{2.5}$ concentrations were summarized from the predicted daily concentrations. For human exposure assessment, population-weighted $PM_{2.5}$ concentrations were calculated on the national and regional levels (van Donkelaar et al., 2015).

$$P_{PW} = \sum_{i=1}^{N} (P_i \times C_i) \Big/ \sum_{i=1}^{N} P_i \tag{8}$$

where P_{PW} is the population-weighted $PM_{2.5}$ concentration for a region covering N grid cells; P_i is the population density of grid cell i; and C_i is the $PM_{2.5}$ concentration of grid cell i. The short- and long-term $PM_{2.5}$ exposure levels for the population in China were evaluated.

2.5. Model evaluation

The GW-GBM model was evaluated with cell-based 10-fold cross-validation, where the training cells were randomly partitioned into 10 groups of approximately the same size. The subsequent steps for obtaining the predictions were similar to those of sample-based 10-fold cross-validation mentioned in the "Model Description" section, i.e., the GW-GBM model trained with 9 groups made predictions for the remaining group, which was repeated 10 times to obtain a complete set of predictions. Note that in the model evaluation, the sample-based cross-validation to determine K was conducted for each repeat of the cell-based cross-validation. To show the improvement by integrating the geographically weighted method, a regular GBM model (hereafter referred to as the original GBM model) was also developed and evaluated with the same training dataset. The predictive performances were measured with the root-mean-square error (RMSE) and coefficient of determination (R^2) in the cross-validation.

In order to test the effectiveness of surrogate splits for handling partially missing data in the GW-GBM model, the quarterly and annual averages of $PM_{2.5}$ predictions for all simulation days were compared with those excluding days with missing AOD data. The differences were plotted in maps, and considered as potential estimation bias if the missing AOD data could not be handled by a model.

The spatial variation of the importance of predictor variables for predicting $PM_{2.5}$ concentrations was evaluated. Here the importance of a predictor variable was defined based on the number of times the variable was used for tree splitting and the consequent error reduction in each GW-GBM sub-model (Friedman, 2001). The formulas for the variable importance measures are listed in the Supplement S3. For each sub-model (or predicting cell), the importance measures of all predictor variables were scaled so that their sum was equal to 100 for more intuitive interpretation. The overall importance measures of the GW-GBM model were calculated as the averages over all cells. The GW-GBM model was implemented in R by mainly adapting from package gbm (R Development Core Team, 2015; Ridgeway, 2015).

3. Results

3.1. Predictive performance

On the basis of the cross-validation results (Table 1), the GW-GBM model showed good performance in predicting daily $PM_{2.5}$ concentrations even when AOD data were partially missing ($R^2 = 0.76$, RMSE = 23.0 μg/m3), which was better than the original GBM model ($R^2 = 0.71$, RMSE = 25.3 μg/m3). The R^2 by region and season ranged from 0.21 for the third quarter in Northwest China (due to the relative small number of monitoring sites in that region; Fig. S1) to 0.79 for the first quarter in East China (Table S2). The performance of the GW-GBM model was generally not sensitive to the spatial smoothing kernel types (Table S3), although the bisquare kernel showed slightly better performance than the tricube and Gaussian kernels. Compared to the statistical measures based on daily data, the GW-GBM model showed better performance for $PM_{2.5}$ predictions on monthly, quarterly, and annual levels, with R^2 of 0.84, 0.85, and 0.84, respectively (Fig. 1).

3.2. Spatiotemporal distributions of $PM_{2.5}$ concentrations

As annual population-weighted averages by region (refer to Fig. S1 for the locations of these regions), the highest $PM_{2.5}$ concentrations in 2014 were predicted in North China (77.5 μg/m3), followed by Central China (71.5 μg/m3) (Table 2). These two regions are highly populated with 39.2% of the total population of China. South China consistently showed the lowest $PM_{2.5}$ levels across the year. Seasonally, the highest national average $PM_{2.5}$ concentrations were predicted in the first quarter (86.0 μg/m3), and the lowest in the third quarter (40.1 μg/m3). In the Central and North China, the average daily $PM_{2.5}$ were predicted to be > 100 μg/m3 during the first quarter. $PM_{2.5}$ pollution was much alleviated in the third quarter for most of China, except for the southeast region of North China (including the national capital region of Beijing-Tianjin-Hebei) and deserts in Northwest China (Fig. 2). The predicted spatiotemporal distributions of $PM_{2.5}$ concentrations were generally consistent with the previous studies for China in 2014 (You et al., 2016a, 2016b), though those two studies did not report population-weighted $PM_{2.5}$ concentrations.

3.3. Exposure to ambient $PM_{2.5}$

On the basis of the continuous spatiotemporal prediction of $PM_{2.5}$ concentrations, it was found that 95% of the Chinese population in 2014 lived in areas where the estimated annual mean $PM_{2.5}$ concentration was >35 μg/m3, and 45% of the population was exposed to $PM_{2.5}$>75 μg/m3 for more than 100 days (Fig. 3). The levels of 35 and 75 μg/m3 are based on World Health Organization (WHO)'s annual and 24-h mean interim target 1 (IT1) air quality guidelines, respectively (WHO, 2006). Spatially, South China had the highest percent of population (26%) living in areas meeting the annual IT1, while the lowest levels were in Northeast and Central

Table 1
Predictive performance based on datasets excluding or including the data points with missing AOD values in cross-validation.

	Excluding missing AOD[a]		Including missing AOD[b]	
	GW-GBM	Original GBM	GW-GBM	Original GBM
RMSE (μg/m^3)	24.3	25.5	23.0	25.3
R^2	0.74	0.71	0.76	0.71
Slope	0.75	0.72	0.77	0.71

[a] Summary of the monitoring $PM_{2.5}$: 62.9 ± 47.6 μg/m3 ($\mu \pm \sigma$; n = 37 626).
[b] Summary of the monitoring $PM_{2.5}$: 58.2 ± 47.2 μg/m3 ($\mu \pm \sigma$; n = 103071).

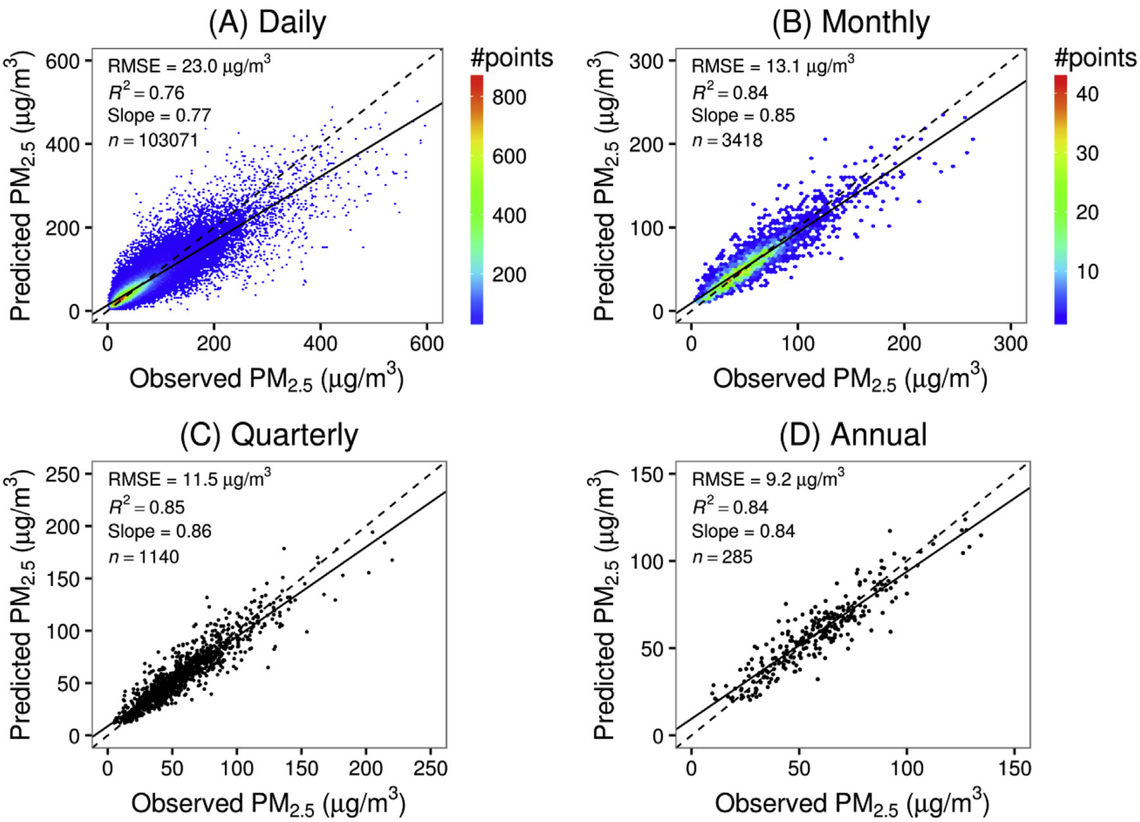

Fig. 1. Evaluation of the predictive performance of the GW-GBM model by using cross-validation at (A) daily, (B) monthly, (C) quarterly, and (D) annual levels.

Table 2
Quarterly and annual averages ± standard deviations of population weighted $PM_{2.5}$ concentrations for each region and the whole nation of China in 2014 ($\mu g/m^3$).

Region[a]	Q1[b]	Q2	Q3	Q4	Annual
Central China	103.2 ± 42.9	62.7 ± 15.0	45.2 ± 10.8	75.4 ± 23.7	71.5 ± 33.5
East China	80.4 ± 39.3	59.9 ± 17.3	41.4 ± 11.8	61.9 ± 19.5	60.8 ± 27.8
North China	106.3 ± 46.2	62.4 ± 18.3	55.2 ± 14.0	86.5 ± 37.7	77.5 ± 37.6
Northeast China	75.0 ± 30.8	39.5 ± 12.9	35.9 ± 15.0	75.3 ± 37.3	56.4 ± 32.1
Northwest China	86.4 ± 27.9	52.4 ± 15.8	38.4 ± 7.0	62.5 ± 16.2	59.8 ± 25.2
South China	54.6 ± 24.6	31.1 ± 8.9	24.3 ± 6.5	48.1 ± 12.2	39.5 ± 19.1
Southwest China	83.4 ± 33.0	47.4 ± 9.9	33.2 ± 6.5	57.4 ± 17.2	55.2 ± 26.7
Nation	86.0 ± 29.0	52.2 ± 8.7	40.1 ± 6.7	68.1 ± 16.9	61.6 ± 24.5

[a] Regions are labelled on Fig. S1.
[b] Q1: January–March; Q2: April–June; Q3: July–September; Q4: October–December.

China (both are 0%). In addition, 33% of the Chinese population was exposed to annual mean $PM_{2.5}$ >70 μg/m3 (twice of the annual IT1). Moreover, Fig. 3B shows the two-way cumulative distributions of $PM_{2.5}$ exposure intensity and duration at the daily level. Not only was the majority of the population exposed to $PM_{2.5}$ exceeding the daily IT1 for most days of the year, but many were also exposed to even higher $PM_{2.5}$ for at least a few days in a year. For instance, 55% of the national population was exposed to $PM_{2.5}$ >150 μg/m3 for more than 10 days in 2014. Note that the personal exposure would likely be more variable than the exposure predicted in this study due to the use of grid-cell $PM_{2.5}$ averages. The personal exposure would be affected by the personal activity pattern, indoor-outdoor air exchange rate, and spatial heterogeneity within each grid cell.

3.4. Estimation bias due to missing AOD retrievals

To evaluate the improvement of model performance with missing data handling, two sets of annual and quarterly averages of $PM_{2.5}$ concentration were calculated by including and excluding GW-GBM predictions for the data points with missing AOD data, and their differences were compared. Without the missing data handling implemented in GW-GBM, the average $PM_{2.5}$ concentrations would have been highly underestimated in Northeast China, and overestimated in South, East, and Northwest China (Fig. 4). The magnitudes of the differences in average $PM_{2.5}$ predictions generally followed the spatiotemporal distributions of the missing rate of AOD coverage (Fig. S2). Higher absolute values of the differences were associated with lower AOD coverage rates. Without missing data handling by GW-GBM model, reduced average $PM_{2.5}$ concentrations (reduced by up to 50 μg/m3) would be reported in Northeast China, especially during the first and fourth quarters when the AOD coverage rates were lower than 20% for a large part of that region. Similarly, the GW-GBM model avoided the potential overestimation (up to >50 μg/m3) of $PM_{2.5}$ concentrations due to AOD data missing in the first and second quarters for South and East China, and in the second quarter for Northwest China (Fig. 4).

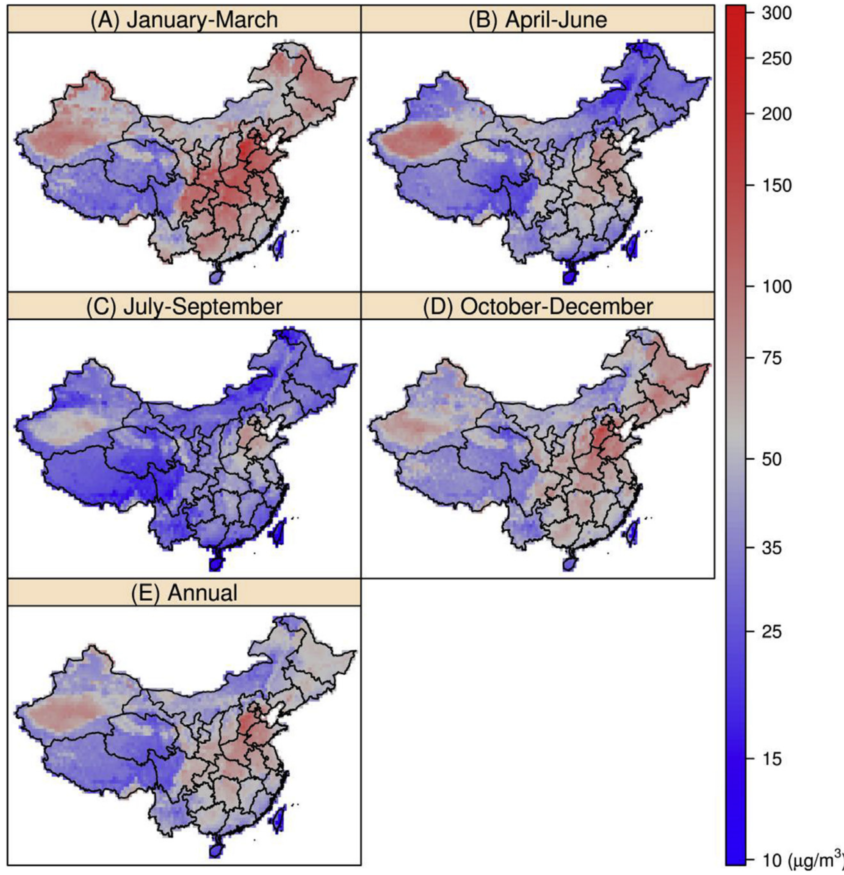

Fig. 2. Spatial distributions of the predicted $PM_{2.5}$ concentrations for China in (A–D) each quarter and (E) the whole year of 2014.

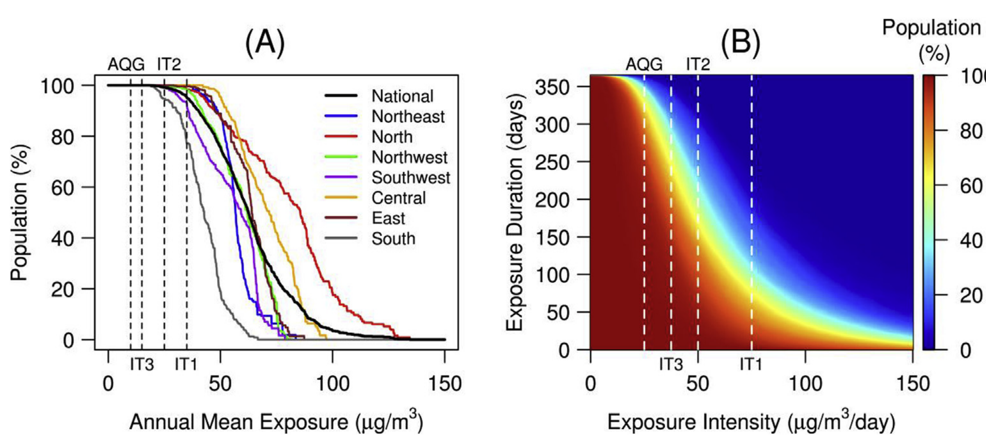

Fig. 3. (A) shows the percent of national or regional population of China in 2014 exposed to $PM_{2.5}$ higher than annual mean levels. (B) presents the percent of nationwide population of China in 2014 exposed to $PM_{2.5}$ higher than daily mean levels for longer than specified days. The WHO air quality guideline (AQG) and interim targets (IT) 1–3 for annual mean (in panal A) and 24-h mean (in panel B) are indicated.

The AOD coverage rates for the overestimated areas within these three regions were generally lower than 30% in the first and second quarters. For other areas with higher AOD coverage (30–90%), the quarterly and annual estimation differences due to missing AOD retrievals were much lower, generally within ±10 μg/m3.

3.5. Variable importance

The three most important predictor variables in the GW-GBM model were day of year (DOY), aerosol optical depth, and atmospheric pressure, with relative importance of 25.7, 13.7, and 13.2, respectively (Table 3). The relative importance of other predictors (e.g., evaporation and temperature) ranged from only 2.4 to 12.5. The spatial distributions of the importance varied greatly among the predictor variables (Table 3 and Fig. S3). DOY played an important role in most areas, especially for Central China. AOD was relatively less important in Central China than other parts of China. The importance measures of atmospheric pressure, wind speed,

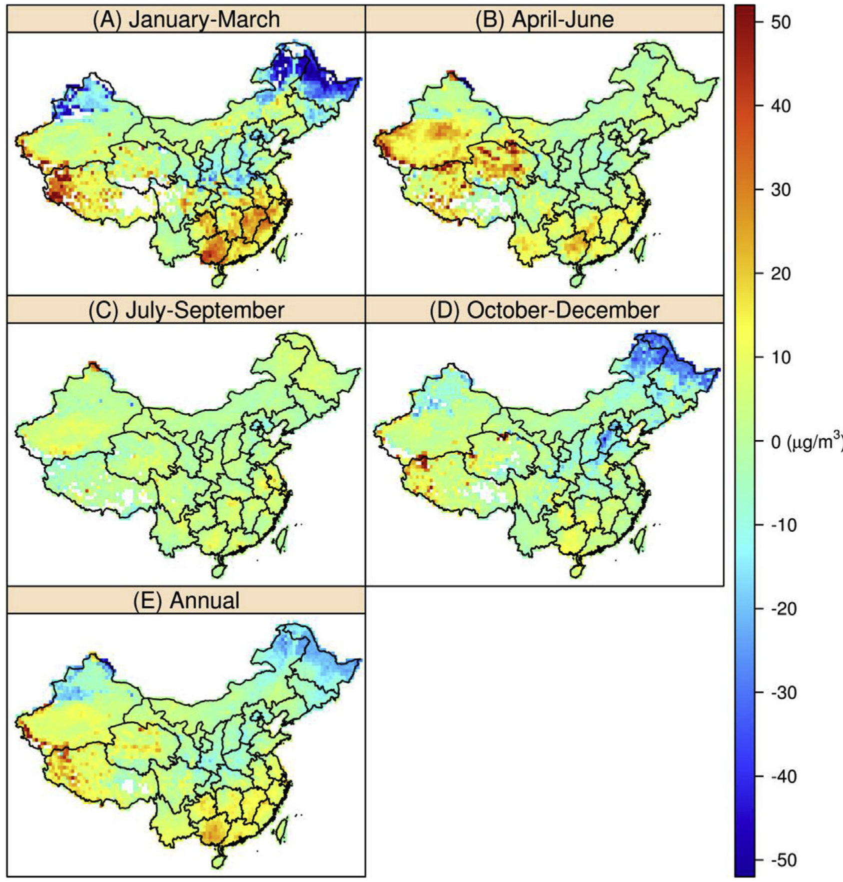

Fig. 4. Estimation bias of average $PM_{2.5}$ concentrations due to missing AOD retrievals for (A–D) each quarter and (E) the whole year of 2014 in China. The estimation bias is the difference between the average of all predicted daily $PM_{2.5}$ concentrations and the average of those with AOD retrievals. Areas with no AOD retrievals during the study periods are not included (blank areas within the study domain).

Table 3
Average variable importance in the GW-GBM model for each region of China.

Region[a]	DOY[b]	AOD	PRS	TEM	WIN	EVP	RHU	SSD	PRE
Central China	42.6	6.7	9.1	10.0	4.9	8.5	7.6	6.1	4.6
East China	36.1	7.3	9.7	12.3	6.1	8.5	7.5	7.8	4.8
North China	22.0	12.3	12.4	15.1	8.4	11.7	7.8	8.5	1.8
Northeast China	22.8	10.5	7.5	17.5	11.9	11.0	9.7	7.8	1.4
Northwest China	22.2	18.2	15.0	12.9	11.0	5.9	6.5	6.9	1.4
South China	29.2	8.1	11.1	12.5	10.9	6.6	12.9	5.0	3.9
Southwest China	27.7	14.9	16.3	8.4	12.6	6.9	5.4	4.6	3.2
Nation	25.7	13.7	13.2	12.5	10.4	8.1	7.4	6.6	2.4

[a] Regions are labelled on Fig. S1.
[b] Variable acronyms: Day of Year (DOY), Aerosol Optical Depth (AOD), Atmospheric Pressure (PRS), Air Temperature (TEM), Wind Speed (WIN), Evaporation (EVP), Relative Humidity (RHU), Sunshine Duration (SSD), and Precipitation (PRE). Please see Fig. S3 for the detailed spatial distributions of variable importance.

and sunshine duration were relatively higher in Northwest China and Tibetan Plateau than in other regions. Air temperature exhibited high importance in Northeast China and a coastal part of South China. The North China Plain (with notoriously severe $PM_{2.5}$ pollution) showed higher importance of evaporation and sunshine duration than other regions. The importance measures of relative humidity and precipitation were relatively higher in South and East China, respectively.

4. Discussion

The GW-GBM model showed good performance in predicting continuous spatiotemporal $PM_{2.5}$ concentrations in China. According to the values of R^2, the performance of the GW-GBM ($R^2 = 0.76$) was better than a previous national study with $R^2 = 0.64$ (Ma et al., 2014), a regional study in the North China Plain with $R^2 = 0.61$ using 10-fold leave-10%-cities-out cross-validation (Lv et al., 2016), and other previous studies (Table S4). These studies employed artificial neural network, Bayesian hierarchical model, geographically weighted regression, and mixed-effects models. It is worthy to note that, besides the model algorithms and predictor variables, validation strategies also affected the resulting values of statistical measures for model performance. For cross-validation, input data could be partitioned by data points, monitoring sites, or grid cells, which were named as sample-, site-, or cell-based cross-validation, respectively.

In this study cell-based 10-fold cross-validation was used, where the training cells are partitioned into 10 groups. In another national study, Ma et al. (2016a) used sample-based cross-validation as indicated in their later study (Ma et al., 2016b), where the samples of data points were partitioned into 10 groups, and reported a higher R^2 of 0.79. In this study when missing-AOD data points were excluded (to be comparable with the previous studies), the sample- and site-based cross-validations resulted in much better performance, according to statistical measures ($R^2 = 0.88$ and 0.87, respectively), than the cell-based cross-validation ($R^2 = 0.74$) (Table S5). This was probably due to higher correlation between training and predicting datasets for the sample-/site-based than the cell-based cross-validation. Since the main purpose of the models was to predict $PM_{2.5}$ concentrations in unmonitored cells, the training/predicting data partition of the cell-based cross-validation better reflected the relationship between training and predicting data for real prediction. Moreover, a higher density of monitoring sites was available in urban areas, and $PM_{2.5}$ concentrations observed within a city were usually similar to each other. Compared to cell-based cross-validation where virtually one "average" site was considered for each cell, site-based cross-validation might lead to over-optimistic estimation of model performance due to the repeated uses of similar measurements within a cell (Lv et al., 2016).

The geographically weighted method refined the GBM model by explicitly addressing the spatial nonstationarity of the dependence of $PM_{2.5}$ concentrations on predictor variables. It was recognized that the relationship between $PM_{2.5}$ concentrations and AOD was spatially nonstationary, especially across a large region (Paciorek and Liu, 2009). Also, the spatial nonstationarity was suggested by the spatial variability on the relative importance of predictor variables across China (Table 3, Fig. S3). The spatial nonstationarity between $PM_{2.5}$ concentrations and AOD was partially addressed by the meteorological variables. Moreover, the geographically weighted method implemented smoothing kernels to screen quasi-stationary areas and to smooth transitions between nonstationary areas. Although the spatial nonstationarity could be addressed by including spatial coordinates as predictor variables in the model, apparent artificial strips emerged in the predicted spatial distributions of $PM_{2.5}$ concentrations (Fig. S4). Furthermore, it is also important to address temporal nonstationarity between $PM_{2.5}$ concentrations and AOD (Kloog et al., 2011). With sufficient computing resources in the future, spatiotemporal smoothing kernels may be implemented in the GW-GBM model to address spatial and temporal nonstationarity simultaneously. Note that the GW-GBM model consists of an ensemble of GW-GBM sub-models, whose number is proportional to the complexity of smoothing kernels implemented, thus it is much more computationally expensive than the original GBM model.

The important predictor variables on the $PM_{2.5}$ concentrations were identified, which provided valuable information for advancing $PM_{2.5}$ prediction in the future. The seasonality of $PM_{2.5}$ concentrations (DOY) derived from the monitoring data was the most important variable. In general, the $PM_{2.5}$ concentrations were relatively low in warm seasons and high in cold seasons, resulting from the seasonality of pollutant emissions and meteorological conditions. The meteorological variables were also highly important for predicting $PM_{2.5}$ concentrations. Air pollutants tended to accumulate when the atmospheric pressure were high and the wind speed were low, which might be enhanced by surface temperature inversion (Zhao et al., 2013). Scavenging by precipitation was important to removal of $PM_{2.5}$ (Tai et al., 2010). While AOD was commonly acknowledged as a good indicator of ambient $PM_{2.5}$, in this study its importance measure was similar to individual meteorological variables. Besides the limited availability of AOD data in the study area (<50% coverage as an annual average), the $PM_{2.5}$-AOD relationship of high uncertainty also degraded the importance of AOD (Paciorek and Liu, 2009). This relationship for example might be affected by the vertical profile of aerosol. Previous studies used the vertical profile simulated by CTMs, e.g., GEOS-Chem, as a scaling factor to estimate the proportion of aerosol depth attributable to ground-level $PM_{2.5}$ (Liu et al., 2004; van Donkelaar et al., 2006). In the future, we also intend to integrate the vertical profile of aerosol into the GW-GBM model for better prediction performance.

Obvious nonlinear and interaction effects of the predictor variables on the $PM_{2.5}$ concentrations were revealed by the partial dependence plots and interaction depths, respectively. A partial dependence plot shows the effect of a variable on the response after accounting for the average effects of all other variables in the model (Supplement S4). Nonlinearity means a nonlinear relationship between a predictor variable and $PM_{2.5}$ concentrations. Interaction is used when the effects of multiple predictor variables on $PM_{2.5}$ concentrations are not equal to the sum of their individual effects. In the GBM or GW-GBM model, while a single decision tree cannot produce nonlinearity, a combination of hundreds or thousands of shrunken trees can fit a nonlinear function (Eq. (7)). The partial dependence plots of the original GBM model reflect the overall nonlinear relationships of the $PM_{2.5}$ concentrations with a few predictor variables (Fig. S5). For example, the partial dependence of $PM_{2.5}$ concentrations on evaporation initially decreased quickly along with the increase of evaporation and then leveled off. In addition, a GW-GBM model consisting of tree stubs indicated no interaction effect, and deep tree depth indicated strong interaction effects. In this study, the complex tree structures (interaction or tree depth: 8.0 ± 2.4) of the fitted GW-GBM model suggest strong interaction effects between the predictor variables on the $PM_{2.5}$ concentrations. Therefore, additive or linear structures were inadequate for modelling $PM_{2.5}$ concentrations.

The GW-GBM model improved the prediction capability for $PM_{2.5}$ by handling incomplete input data, particularly partially missing AOD retrievals. In Northeast China, for example, AOD retrievals tended to be missing in the first and fourth quarters (Fig. S2), which might be related to high reflectance of snow. At the same time, high $PM_{2.5}$ concentrations were also predicted (Table 2). More fuel was combusted for heating in cold days, usually accompanied with snow cover (Xu et al., 2011), resulting in higher $PM_{2.5}$ concentrations compared to warmer days when AOD retrievals were available. In contrast, AOD retrievals in South China tended to be missing in the first and second quarters (Fig. S2), which might be due to cloud cover associated with rain. Compared to sunny days, $PM_{2.5}$ concentrations in rainy days were lower because of rain scavenging. If a model did not generate $PM_{2.5}$ predictions for the data points with missing AOD data during those months (Ma et al., 2016a), it would generate biased estimates of the pollution and exposure level in terms of average concentrations (Fig. 4). Since missing AOD data are frequently observed during highly polluted periods in China, missing data handling is very important for accurate $PM_{2.5}$ predictions in China.

The GW-GBM model equipped with surrogate splits was superior to traditional statistical models in handling missing data for $PM_{2.5}$ prediction. Traditional statistical models were generally incapable of making predictions for the modeling time nodes when input data were partially missing. Thus, these models relied on other methods to fill the data gaps. In previous studies, data fusion or interpolation were conducted to fill AOD gaps (Lv et al., 2016; Nguyen et al., 2012; Xu et al., 2015), where AOD were fused from multiple data sources and/or geostatistical interpolation (e.g., Kriging) was used to fill the missing values. Another method was to interpolate $PM_{2.5}$ values estimated for the data points with AOD retrievals to those with missing values through smoothing such as thin plate spline (Kloog et al., 2011). However, change-of-support or uncertainty propagation might emerge as a result, and the interpolation tended to smooth spatial variations of AOD or $PM_{2.5}$. To avoid these problems, the GW-GBM model built surrogate splits based on the patterns learned from the training data with AOD retrieved from the Aqua satellite only. Surrogate splits utilized correlations of AOD values with the other predictor variables to reduce the loss of information due to missing values (Hastie et al., 2009). As the AOD missing rates were considerable in $PM_{2.5}$ prediction, it was better to use a model that could handle missing data than to use models that relied on additional missing data filling methods.

5. Conclusions

A spatially explicit machine learning algorithm, named GW-GBM, was developed to predict the spatiotemporal distributions of continuous daily $PM_{2.5}$ concentrations in China. All predictor variables of the model are readily available from public data sources. The GW-GBM model addressed spatial nonstationarity of the dependence of $PM_{2.5}$ on environmental conditions, considerably improving the predictive performance. The GW-GBM model revealed interaction and nonlinear effects that are underrepresented by conventional statistical models. The GW-GBM model also overcame the estimation bias of $PM_{2.5}$ concentrations due to missing AOD retrievals, which tends to bias the exposure analyses. This study provided reliable data, such as exposure intensity and duration, for assessing acute human health effects of $PM_{2.5}$ exposure in China. In the future, comparative analyses with epidemiological data in China are expected to provide helpful information for refining exposure-response curves at higher $PM_{2.5}$ concentrations.

Acknowledgements

This work was supported by the National Natural Science Foundation of China [21607127], and the Key Research and Development Program of Ministry of Science and Technology of China [2016YFC020710].

Appendix A. Supplementary data

Supplementary data related to this article can be found at http://dx.doi.org/10.1016/j.atmosenv.2017.02.023.

References

Apte, J.S., Marshall, J.D., Cohen, A.J., Brauer, M., 2015. Addressing global mortality from ambient $PM_{2.5}$. Environ. Sci. Technol. 49, 8057–8066.
Bey, I., Jacob, D.J., Yantosca, R.M., Logan, J.A., Field, B.D., Fiore, A.M., Li, Q., Liu, H.Y., Mickley, L.J., Schultz, M.G., 2001. Global modeling of tropospheric chemistry with assimilated meteorology: model description and evaluation. J. Geophys. Res. Atmos. 106, 23073–23095.
Brauer, M., Amann, M., Burnett, R.T., Cohen, A., Dentener, F., Ezzati, M., Henderson, S.B., Krzyzanowski, M., Martin, R.V., Van Dingenen, R., van Donkelaar, A., Thurston, G.D., 2012. Exposure assessment for estimation of the Global Burden of Disease attributable to outdoor air pollution. Environ. Sci. Technol. 46, 652–660.
Brauer, M., Freedman, G., Frostad, J., van Donkelaar, A., Martin, R.V., Dentener, F., Dingenen, R.v., Estep, K., Amini, H., Apte, J.S., Balakrishnan, K., Barregard, L., Broday, D., Feigin, V., Ghosh, S., Hopke, P.K., Knibbs, L.D., Kokubo, Y., Liu, Y., Ma, S., Morawska, L., Sangrador, J.L.T., Shaddick, G., Anderson, H.R., Vos, T., Forouzanfar, M.H., Burnett, R.T., Cohen, A., 2016. Ambient air pollution exposure estimation for the Global Burden of Disease 2013. Environ. Sci. Technol. 50, 79–88.
Breiman, L., 2001. Statistical modeling: the two cultures. Stat. Sci. 16, 199–215.
Breiman, L., Friedman, J., Stone, C.J., Olshen, R.A., 1984. Classification and Regression Trees. edˆeds. New York: Wadsworth.
Brunsdon, C., Fotheringham, A.S., Charlton, M.E., 1996. Geographically weighted regression: a method for exploring spatial nonstationarity. Geogr. Anal. 28, 281–298.
Burnett, R.T., Pope 3rd, C.A., Ezzati, M., Olives, C., Lim, S.S., Mehta, S., Shin, H.H., Singh, G., Hubbell, B., Brauer, M., Anderson, H.R., Smith, K.R., Balmes, J.R., Bruce, N.G., Kan, H., Laden, F., Pruss-Ustun, A., Turner, M.C., Gapstur, S.M., Diver, W.R., Cohen, A., 2014. An integrated risk function for estimating the global burden of disease attributable to ambient fine particulate matter exposure. Environ. Health Perspect. 122, 397–403.
Deutsch, C.V., Journel, A.G., 1998. GSLIB Geostatistical Software Library and User's Guide. ˆeds, second ed. Oxford University Press, New York.
Di, Q., Kloog, I., Koutrakis, P., Lyapustin, A., Wang, Y., Schwartz, J., 2016. Assessing $PM_{2.5}$ exposures with high spatiotemporal resolution across the continental United States. Environ. Sci. Technol. 50, 4712–4721.
Dockery, D.W., Pope, C.A., Xu, X., Spengler, J.D., Ware, J.H., Fay, M.E., Ferris, B.G.J., Speizer, F.E., 1993. An association between air pollution and mortality in six U.S. cities. N. Engl. J. Med. 329, 1753–1759.
Elith, J., Leathwick, J.R., Hastie, T., 2008. A working guide to boosted regression trees. J. Anim. Ecol. 77, 802–813.
Friedman, J.H., 2001. Greedy function approximation: a gradient boosting machine. Ann. Stat. 29, 1189–1232.
Friedman, J.H., 2002. Stochastic gradient boosting. Comput. Stat. Data Anal. 38, 367–378.
Geng, G., Zhang, Q., Martin, R.V., van Donkelaar, A., Huo, H., Che, H., Lin, J., He, K., 2015. Estimating long-term $PM_{2.5}$ concentrations in China using satellite-based aerosol optical depth and a chemical transport model. Remote Sens. Environ. 166, 262–270.
Hastie, T., Tibshirani, R., Friedman, J., 2009. The Elements of Statistical Learning: Data Mining, Inference, and Prediction. ˆeds, second ed. Springer-Verlag, New York.
Jacob, D., 1999. Introduction to Atmospheric Chemistry Ed. ˆeds. Princeton University Press, Princeton, New Jersey.
Jarvis, A., Reuter, H.I., Nelson, A., Guevara, E., 2008. Hole-filled seamless SRTM data V4.1. International Centre for Trop.ical Agric.ulture (CIAT). http://srtm.csi.cgiar.org.
Keller, J.P., Olives, C., Kim, S.Y., Sheppard, L., Sampson, P.D., Szpiro, A.A., Oron, A.P., Lindstrom, J., Vedal, S., Kaufman, J.D., 2015. A unified spatiotemporal modeling approach for predicting concentrations of multiple air pollutants in the multiethnic study of atherosclerosis and air pollution. Environ. Health Perspect. 123, 301–309.
Kloog, I., Koutrakis, P., Coull, B.A., Lee, H.J., Schwartz, J., 2011. Assessing temporally and spatially resolved PM2.5 exposures for epidemiological studies using satellite aerosol optical depth measurements. Atmos. Environ. 45, 6267–6275.
Lai, H.-K., Hedley, A.J., Thach, T.Q., Wong, C.-M., 2013. A method to derive the relationship between the annual and short-term air quality limits—analysis using the WHO Air Quality Guidelines for health protection. Environ. Int. 59, 86–91.
Levy, R.C., Mattoo, S., Munchak, L.A., Remer, L.A., Sayer, A.M., Patadia, F., Hsu, N.C., 2013. The Collection 6 MODIS aerosol products over land and ocean. Atmos. Meas. Tech. 6, 2989–3034.
Liu, Y., Park, R.J., Jacob, D.J., Li, Q., Kilaru, V., Sarnat, J.A., 2004. Mapping annual mean ground-level $PM_{2.5}$ concentrations using Multiangle Imaging Spectroradiometer aerosol optical thickness over the contiguous United States. J. Geophys. Res. Atmos. 109, 1–10.
Lv, B., Hu, Y., Chang, H.H., Russell, A.G., Bai, Y., 2016. Improving the accuracy of daily $PM_{2.5}$ distributions derived from the fusion of ground-level measurements with aerosol optical depth observations, a case study in North China. Environ. Sci. Technol. 50, 4752–4759.
Lyapustin, A., Wang, Y., Laszlo, I., Kahn, R., Korkin, S., Remer, L., Levy, R., Reid, J.S., 2011. Multiangle implementation of atmospheric correction (MAIAC): 2. Aerosol algorithm. J. Geophys. Res. Atmos. 116.
Ma, Z., Hu, X., Huang, L., Bi, J., Liu, Y., 2014. Estimating ground-level $PM_{2.5}$ in China using satellite remote sensing. Environ. Sci. Technol. 48, 7436–7444.
Ma, Z., Hu, X., Sayer, A.M., Levy, R., Zhang, Q., Xue, Y., Tong, S., Bi, J., Huang, L., Liu, Y., 2016a. Satellite-based spatiotemporal trends in $PM_{2.5}$ concentrations: China, 2004-2013. Environ. Health Perspect. 124, 184–192.
Ma, Z., Liu, Y., Zhao, Q., Liu, M., Zhou, Y., Bi, J., 2016b. Satellite-derived high resolution $PM_{2.5}$ concentrations in Yangtze River Delta Region of China using improved linear mixed effects model. Atmos. Environ. 133, 156–164.
Madaniyazi, L., Nagashima, T., Guo, Y., Yu, W., Tong, S., 2015. Projecting fine particulate matter-related mortality in East China. Environ. Sci. Technol. 49, 11141–11150.
MEPC, 2015. Air Quality Daily Report.: Ministry of Environmental Protection of the People's Republic of China. http://datacenter.mep.gov.cn/.
Naghavi, M., Wang, H., Lozano, R., Davis, A., Liang, X., Zhou, M., Vollset, S.E., Ozgoren, A.A., Abdalla, S., Abd-Allah, F., Aziz, M.I.A., Abera, S.F., Aboyans, V., Abraham, B., Abraham, J.P., Abuabara, K.E., Abubakar, I., Abu-Raddad, L.J., Abu-Rmeileh, N.M.E., Achoki, T., Adelekan, A., Ademi, Z.N., Adofo, K., Adou, A.K., Adsuar, J.C., Aernlov, J., Agardh, E.E., Akena, D., Al Khabouri, M.J., Alasfoor, D., Albittar, M., Alegretti, M.A., Aleman, A.V., Alemu, Z.A., Alfonso-Cristancho, R., Alhabib, S., Ali, M.K., Ali, R., Alla, F., Al Lami, F., Allebeck, P., AlMazroa, M.A., Salman, R.A.-S., Alsharif, U., Alvarez, E., Alviz-Guzman, N., Amankwaa, A.A., Amare, A.T., Ameli, O., Amini, H., Ammar, W., Anderson, H.R., Anderson, B.O., Antonio, C.A.T., Anwari, P., Apfel, H., Cunningham, S.A., Arsenijevic, V.S.A., Al, A., Asad, M.M., Asghar, R.J., Assadi, R., Atkins, L.S., Atkinson, C., Badawi, A., Bahit, M.C., Bakfalouni, T., Balakrishnan, K., Balalla, S., Banerjee, A., Barber, R.M., Barker-Collo, S.L., Barquera, S., Barregard, L., Barrero, L.H., Barrientos-Gutierrez, T., Basu, A., Basu, S., Basulaiman, M.O., Beardsley, J., Bedi, N., Beghi, E., Bekele, T., Bell, M.L., Benjet, C., Bennett, D.A., Bensenor, I.M., Benzian, H., Bertozzi-Villa, A., Beyene, T.J., Bhala, N., Bhalla, A., Bhutta, Z.A., Bikbov, B., Bin Abdulhak, A., Biryukov, S., Blore, J.D., Blyth, F.M., Bohensky, M.A., Borges, G., Bose, D., Boufous, S., Bourne, R.R., Boyers, L.N., Brainin, M., Brauer, M., Brayne, C.E.G., Brazinova, A., Breitborde, N., Brenner, H., Briggs, A.D.M., Brown, J.C., Brugha, T.S., Buckle, G.C., Bui, L.N., Bukhman, G., Burch, M., Nonato, I.R.C., Carabin, H., Cardenas, R., Carapetis, J., Carpenter, D.O., Caso, V., Castaneda-Orjuela, C.A., Castro, R.E., Catala-Lopez, F., Cavalleri, F., Chang, J.-C., Charlson, F.C., Che, X., Chen, H., Chen, Y., Chen, J.S., Chen, Z., Chiang, P.P.-C., Chimed-Ochir, O., Chowdhury, R., Christensen, H., Christophi, C.A., Chuang, T.-W., Chugh, S.S., Cirillo, M., Coates, M.M., Coffeng, L.E., Coggeshall, M.S., Cohen, A., Colistro, V., Colquhoun, S.M., Colomar, M., Cooper, L.T., Cooper, C., Coppola, L.M., Cortinovis, M., Courville, K., Cowie, B.C., Criqui, M.H., Crump, J.A., Cuevas-Nasu, L., Leite, I.d.C., Dabhadkar, K.C., Dandona, L., Dandona, R., Dansereau, E., Dargan, P.I., Dayama, A., De la Cruz-Gongora, V., de la Vega, S.F., De Leo, D., Degenhardt, L., del Pozo-Cruz, B., Dellavalle, R.P., Deribe, K., Jarlais, D.C.D., Dessalegn, M., deVeber, G.A., Dharmaratne, S.D., Dherani, M., Diaz-Ortega, J.-L., Diaz-Torne, C., Dicker, D., Ding, E.L., Dokova, K., Dorsey, E.R.,

Driscoll, T.R., Duan, L., Duber, H.C., Durrani, A.M., Ebel, B.E., Edmond, K.M., Ellenbogen, R.G., Elshrek, Y., Ermakov, S.P., Erskine, H.E., Eshrati, B., Esteghamati, A., Estep, K., Fuerst, T., Fahimi, S., Fahrion, A.S., Faraon, E.J.A., Farzadfar, F., Fay, D.F.J., Feigl, A.B., Feigin, V.L., Felicio, M.M., Fereshtehnejad, S.-M., Fernandes, J.G., Ferrari, A.J., Fleming, T.D., Foigt, N., Foreman, K., Forouzanfar, M.H., Fowkes, F.G.R., Fra Paleo, U., Franklin, R.C., Futran, N.D., Gaffikin, L., Gambashidze, K., Gankpe, F.G., Garcia-Guerra, F.A., Garcia, A.C., Geleijnse, J.M., Gessner, B.D., Gibney, K.B., Gillum, R.F., Gilmour, S., Abdelmageem, I., Ginawi, M., Giroud, M., Glaser, E.L., Goenka, S., Dantes, H.G., Gona, P., Gonzalez-Medina, D., Guinovart, C., Gupta, R., Gupta, R., Gosselin, R.A., Gotay, C.C., Goto, A., Gowda, H.N., Graetz, N., Greenwell, K.F., Gugnani, H.C., Gunnell, D., Gutierrez, R.A., Haagsma, J., Hafezi-Nejad, N., Hagan, H., Hagstromer, M., Halasa, Y.A., Hamadeh, R.R., Hamavid, H., Hammami, M., Hancock, J., Hankey, G.J., Hansen, G.M., Harb, H.L., Harewood, H., Haro, J.M., Havmoeller, R., Hay, R.J., Hay, S.I., Hedayati, M.T., Pi, I.B.H., Heuton, K.R., Heydarpour, P., Higashi, H., Hijar, M., Hoek, H.W., Hoffman, H.J., Hornberger, J.C., Hosgood, H.D., Hossain, M., Hotez, P.J., Hoy, D.G., Hsairi, M., Hu, G., Huang, J.J., Huffman, M.D., Hughes, A.J., Husseini, A., Huynh, C., Iannarone, M., Iburg, K.M., Idrisov, B.T., Ikeda, N., Innos, K., Inoue, M., Islami, F., Ismayilova, S., Jacobsen, K.H., Jassal, S., Jayaraman, S.P., Jensen, P.N., Jha, V., Jiang, G., Jiang, Y., Jonas, J.B., Joseph, J., Juel, K., Kabagambe, E.K., Kan, H., Karch, A., Karimkhani, C., Karthikeyan, G., Kassebaum, N., Kaul, A., Kawakami, N., Kazanjan, K., Kazi, D.S., Kemp, A.H., Kengne, A.P., Keren, A., Kereselidze, M., Khader, Y.S., Khalifa, S.E.A.H., Khan, E.A., Khan, G., Khang, Y.-H., Kieling, C., Kinfu, Y., Kinge, J.M., Kim, D., Kim, S., Kivipelto, M., Knibbs, L., Knudsen, A.K., Kokubo, Y., Kosen, S., Kotagal, M., Kravchenko, M.A., Krishnaswami, S., Krueger, H., Defo, B.K., Kuipers, E.J., Bicer, B.K., Kulkarni, C., Kulkarni, V.S., Kumar, K., Kumar, R.B., Kwan, G.F., Kyu, H., Lai, T., Balaji, A.L., Lalloo, R., Lallukka, T., Lam, H., Lan, Q., Lansingh, V.C., Larson, H.J., Larsson, A., Lavados, P.M., Lawrynowicz, A.E.B., Leasher, J.L., Lee, J.-T., Leigh, J., Leinsalu, M., Leung, R., Levitz, C., Li, B., Li, Y., Li, Y., Liddell, C., Lim, S.S., de Lima, G.M.F., Lind, M.L., Lipshultz, S.E., Liu, S., Liu, Y., Lloyd, B.K., Lofgren, K.T., Logroscino, G., London, S.J., Lortet-Tieulent, J., Lotufo, P.A., Lucas, R.M., Lunevicius, R., Lyons, R.A., Ma, S., Machado, V.M.P., MacIntyre, M.F., Mackay, M.T., MacLachlan, J.H., Magis-Rodriguez, C., Mahdi, A.A., Majdan, M., Malekzadeh, R., Mangalam, S., Mapoma, C.C., Marape, M., Marcenes, W., Margono, C., Marks, G.B., Marzan, M.B., Masci, J.R., Mashal, M.T.Q., Masiye, F., Mason-Jones, A.J., Matzopolous, R., Mayosi, B.M., Mazorodze, T.T., McGrath, J.J., McKay, A.C., McKee, M., McLain, A., Meaney, P.A., Mehndiratta, M.M., Mejia-Rodriguez, F., Melaku, Y.A., Meltzer, M., Memish, Z.A., Mendoza, W., Mensah, G.A., Meretoja, A., Mhimbira, F.A., Miller, T.R., Mills, E.J., Misganaw, A., Mishra, S.K., Mock, C.N., Moffitt, T.E., Ibrahim, N.M., Mohammad, K.A., Mokdad, A.H., Mola, G.L., Monasta, L., Monis, J.d.l.C., Hernandez, J.C.M., Montico, M., Montine, T.J., Mooney, M.D., Moore, A.R., Moradi-Lakeh, M., Moran, A.E., Mori, R., Moschandreas, J., Moturi, W.N., Moyer, M.L., Mozaffarian, D., Mueller, U.O., Mukaigawara, M., Mullany, E.C., Murray, J., Mustapha, A., Naghavi, P., Naheed, A., Naidoo, K.S., Naldi, L., Nand, D., Nangia, V., Narayan, K.M.V., Nash, D., Nasher, J., Nejjari, C., Nelson, R.G., Neuhouser, M., Neupane, S.P., Newcomb, P.A., Newman, L., Newton, C.R., Ng, M., Ngalesoni, F.N., Nguyen, G., Nhung Thi Trang, N., Nisar, M.I., Nolte, S., Norheim, O.F., Norman, R.E., Norrving, B., Nyakarahuka, L., Odell, S., O'Donnell, M., Ohkubo, T., Ohno, S.L., Olusanya, B.O., Omer, S.B., Opio, J.N., Orisakwe, O.E., Ortblad, K.F., Ortiz, A., Otayza, M.L.K., Pain, A.W., Pandian, J.D., Panelo, C.I., Panniyammakal, J., Papachristou, C., Paternina Caicedo, A.J., Patten, S.B., Patton, G.C., Paul, V.K., Pavlin, B., Pearce, N., Pellegrini, C.A., Pereira, D.M., Peresson, S.C., Perez-Padilla, R., Perez-Ruiz, F.P., Perico, N., Pervaiz, A., Pesudovs, K., Peterson, C.B., Petzold, M., Phillips, B.K., Phillips, D.E., Phillips, M.R., Plass, D., Piel, F.B., Poenaru, D., Polinder, S., Popova, S., Poulton, R.G., Pourmalek, F., Prabhakaran, D., Qato, D., Quezada, A.D., Quistberg, D.A., Rabito, F., Rafay, A., Rahimi, K., Rahimi-Movaghar, V., Rahman, S.U.R., Raju, M., Rakovac, I., Rana, S.M., Refaat, A., Remuzzi, G., Ribeiro, A.L., Ricci, S., Riccio, P.M., Richardson, L., Richardus, J.H., Roberts, B., Roberts, D.A., Robinson, M., Roca, A., Rodriguez, A., Rojas-Rueda, D., Ronfani, L., Room, R., Roth, G.A., Rothenbacher, D., Rothstein, D.H., Rowley, J.T., Roy, N., Ruhago, G.M., Rushton, L., Sambandam, S., Soreide, K., Saeedi, M.Y., Saha, S., Sahathevan, R., Sahraian, M.A., Sahle, B.W., Salomon, J.A., Salvo, D., Samonte, G.M.J., Sampson, U., Sanabria, J.R., Sandar, L., Santos, I.S., Satpathy, M., Sawhney, M., Saylan, M., Scarborough, P., Schoettker, B., Schmidt, J.C., Schneider, I.J.C., Schumacher, A.E., Schwebel, D.C., Scott, J.G., Sepanlou, S.G., Servan-Mori, E.E., Shackelford, K., Shaheen, A., Shahraz, S., Shakh-Nazarova, M., Shangguan, S., She, J., Sheikhbahaei, S., Shepard, D.S., Shibuya, K., Shinohara, Y., Shishani, K., Shiue, I., Shivakoti, R., Shrime, M.G., Sigfusdottir, I.D., Silberberg, D.H., Silva, A.P., Simard, E.P., Sindi, S., Singh, J.A., Singh, L., Sioson, E., Skirbekk, V., Sliwa, K., So, S., Soljak, M., Soneji, S., Soshnikov, S.S., Sposato, L.A., Sreeramareddy, C.T., Stanaway, J.R.D., Stathopoulou, V.K., Steenland, K., Stein, C., Steiner, C., Stevens, A., Stoeckl, H., Straif, K., Stroumpoulis, K., Sturua, L., Sunguya, B.F., Swaminathan, S., Swaroop, M., Sykes, B.L., Tabb, K.M., Takahashi, K., Talongwa, R.T., Tan, F., Tanne, D., Tanner, M., Tavakkoli, M., Ao, B.T., Teixeira, C.M., Templin, T., Tenkorang, E.Y., Terkawi, A.S., Thomas, B.A., Thorne-Lyman, A.L., Thrift, A.G., Thurston, G.D., Tillmann, T., Tirschwell, D.L., Tleyjeh, I.M., Tonelli, M., Topouzis, F., Towbin, J.A., Toyoshima, H., Traebert, J., Tran, B.X., Truelsen, T., Trujillo, U., Trillini, M., Dimbuene, Z.T., Tsilimbaris, M., Tuzcu, E.M., Ubeda, C., Uchendu, U.S., Ukwaja, K.N., Undurraga, E.A., Vallely, A.J., van de Vijver, S., van Gool, C.H., Varakin, Y.Y., Vasankari, T.J., Vasconcelos, A.M.N., Vavilala, M.S., Venketasubramanian, N., Vijayakumar, L., Villalpando, S., Violante, F.S., Vlassov, V.V., Wagner, G.R., Waller, S.G., Wang, J., Wang, L., Wang, X., Wang, Y., Warouw, T.S., Weichenthal, S., Weiderpass, E., Weintraub, R.G., Wenzhi, W., Werdecker, A., Wessells, K.R.R., Westerman, R., Whiteford, H.A., Wilkinson, J.D., Williams, T.N., Woldeyohannes, S.M., Wolfe, C.D.A., Wolock, T.M., Woolf, A.D., Wong, J.Q., Wright, J.L., Wulf, S., Wurtz, B., Xu, G., Yang, Y.C., Yano, Y., Yatsuya, H., Yip, P., Yonemoto, N., Yoon, S.-J., Younis, M., Yu, C., Jin, K.Y., Zaki, M.E.S., Zamakhshary, M.F., Zeeb, H., Zhang, Y., Zhao, Y., Zheng, Y., Zhu, J., Zhu, S., Zonies, D., Zou, X.N., Zunt, J.R., Vos, T., Lopez, A.D., Murray, C.J.L., Colla, G.B.D.M.C.D., 2015. Global, regional, and national age-sex specific all-cause and cause-specific mortality for 240 causes of death, 1990-2013: a systematic analysis for the Global Burden of Disease Study 2013. Lancet 385, 117–171.

NBSC, 2013. China Energy Statistical Yearbook of 2013. in: Energy statistics division of national bureau of statistics of the People's Republic of China. In: National Bureau of Statistics of the People's Republic of China.

NBSC, 2015. China Energy Statistical Yearbook of 2014. in: Energy statistics division of national bureau of statistics of the People's republic of China. In: National Bureau of Statistics of the People's Republic of China.

Nguyen, H., Cressie, N., Braverman, A., 2012. Spatial statistical data fusion for remote sensing applications. J. Am. Stat. Assoc. 107, 1004–1018.

Paciorek, C.J., Liu, Y., 2009. Limitations of remotely sensed aerosol as a spatial proxy for fine particulate matter. Environ. Health Perspect. 117, 904–909.

Pope III, C.A., Burnett, R.T., Turner, M.C., Cohen, A., Krewski, D., Jerrett, M., Gapstur, S.M., Thun, M.J., 2011. Lung cancer and cardiovascular disease mortality associated with ambient air pollution and cigarette smoke: shape of the exposure-response relationships. Environ. Health Perspect. 119, 1616–1621.

Puett, R.C., Hart, J.E., Yanosky, J.D., Paciorek, C., Schwartz, J., Suh, H., Speizer, F.E., Laden, F., 2009. Chronic fine and coarse particulate exposure, mortality, and coronary heart disease in the Nurses' Health Study. Environ. Health Perspect. 117, 1697–1701.

R Development Core Team, 2015. R: a Language and Environment for Statistical Computing. R Foundation for Statistical Computing, Vienna, Austria. http://www.R-project.org.

Reid, C.E., Jerrett, M., Petersen, M.L., Pfister, G.G., Morefield, P.E., Tager, I.B., Raffuse, S.M., Balmes, J.R., 2015. Spatiotemporal prediction of fine particulate matter during the 2008 Northern California wildfires using machine learning. Environ. Sci. Technol. 49, 3887–3896.

RESDC, 2014. Gridded population of China in 2010. Resources and Environmental Sciences, Chinese Academy of Sciences. http://www.resdc.cn.

Rich, D.Q., Liu, K., Zhang, J., Thurston, S.W., Stevens, T.P., Pan, Y., Kane, C., Weinberger, B., Ohman-Strickland, P., Woodruff, T.J., 2015. Differences in birth weight associated with the 2008 Beijing Olympic air pollution reduction: results from a natural experiment. Environ. Health Perspect. 123, 880–887.

Ridgeway, G., 2015. Gbm: Generalized Boosted Regression Models. R Package Version 2.1.1. Update. https://CRAN.R-project.org/package=gbm.

Shang, Y., Sun, Z., Cao, J., Wang, X., Zhong, L., Bi, X., Li, H., Liu, W., Zhu, T., Huang, W., 2013. Systematic review of Chinese studies of short-term exposure to air pollution and daily mortality. Environ. Int. 54, 100–111.

SCPRC, 2013. Air Pollution Prevention and Control Action Plan. China Clean Air Updates. State Council of the People's Republic of China, Beijing. http://www.cleanairchina.org/file/loadFile/27.html.

Tai, A.P.K., Mickley, L.J., Jacob, D.J., 2010. Correlations between fine particulate matter (PM2.5) and meteorological variables in the United States: implications for the sensitivity of PM2.5 to climate change. Atmos. Environ. 44, 3976–3984.

van Donkelaar, A., Martin, R.V., Park, R.J., 2006. Estimating ground-level $PM_{2.5}$ using aerosol optical depth determined from satellite remote sensing. J. Geophys. Res. Atmos. 111, 1–10.

van Donkelaar, A., Martin, R.V., Brauer, M., Kahn, R., Levy, R., Verduzco, C., Villeneuve, P.J., 2010. Global estimates of ambient fine particulate matter concentrations from satellite-based aerosol optical depth: development and application. Environ. Health Perspect. 118, 847–855.

van Donkelaar, A., Martin, V., Brauer, M., Boys, L., 2015. Use of satellite observations for long-term exposure assessment of global concentrations of fine particulate matter. Environ. Health Perspect. 123, 135–143.

van Donkelaar, A., Martin, R.V., Brauer, M., Hsu, N.C., Kahn, R.A., Levy, R.C., Lyapustin, A., Sayer, A.M., Winker, D.M., 2016. Global estimates of fine particulate matter using a combined geophysical-statistical method with information from satellites, models, and monitors. Environ. Sci. Technol. 50, 3762–3772.

WHO, 2006. Air Quality Guidelines: Global Update 2005. Particulate Matter, Ozone, Nitrogen Dioxide and Sulfur Dioxide. World Health Organization. http://www.euro.who.int/__data/assets/pdf_file/0005/78638/E90038.pdf.

Xie, Y., Wang, Y., Zhang, K., Dong, W., Lv, B., Bai, Y., 2015. Daily estimation of ground-level $PM_{2.5}$ concentrations over Beijing using 3 km resolution MODIS AOD. Environ. Sci. Technol. 49, 12280–12288.

Xu, W.Y., Zhao, C.S., Ran, L., Deng, Z.Z., Liu, P.F., Ma, N., Lin, W.L., Xu, X.B., Yan, P., He, X., Yu, J., Liang, W.D., Chen, L.L., 2011. Characteristics of pollutants and their correlation to meteorological conditions at a suburban site in the North China Plain. Atmos. Chem. Phys. 11, 4353–4369.

Xu, H., Guang, J., Xue, Y., de Leeuw, G., Che, Y.H., Guo, J., He, X.W., Wang, T.K., 2015. A consistent aerosol optical depth (AOD) dataset over mainland China by integration of several AOD products. Atmos. Environ. 114, 48–56.

You, W., Zang, Z., Zhang, L., Li, Y., Pan, X., Wang, W., 2016a. National-Scale estimates of ground-level PM2.5 concentration in China using geographically weighted regression based on 3 km resolution MODIS AOD. Remote Sens. 8, 184.

You, W., Zang, Z., Zhang, L., Li, Y., Wang, W., 2016b. Estimating national-scale

ground-level PM25 concentration in China using geographically weighted regression based on MODIS and MISR AOD. Environ. Sci. Pollut. R. 23, 8327–8338.
Zhao, X.J., Zhao, P.S., Xu, J., Meng, W., Pu, W.W., Dong, F., He, D., Shi, Q.F., 2013. Analysis of a winter regional haze event and its formation mechanism in the North China Plain. Atmos. Chem. Phys. 13, 5685–5696.
Zhao, S., Yu, Y., Yin, D., He, J., Liu, N., Qu, J., Xiao, J., 2016. Annual and diurnal variations of gaseous and particulate pollutants in 31 provincial capital cities based on in situ air quality monitoring data from China National Environmental Monitoring Center. Environ. Int. 86, 92–106.